CHAPTER 48

APPLICATION OF A DIGITAL PARTICLE IMAGE VELOCIMETRY (DPIV) SYSTEM TO BREAKING WAVES IN THE SURF ZONE

Kenneth R. Craig II[1] and Robert J. Thieke[2]

BACKGROUND

The modeling of cross-shore and longshore currents in the nearshore region has improved greatly over the past twenty years with accompanying advances in an understanding of the relevant physical processes in shallow water and the surf zone. The empirical guidance provided by numerous laboratory and field experiments has been an essential element in sustaining these advances. However good experimental data are still largely lacking for aspects of these flows, the most notable being the flow in waves following breaking, which coincidentally represents the single most important physical process in the nearshore region.

For the two-dimensional case of waves normally incident on a beach, a variety of techniques have recorded velocities in surf zone flows. Wang, et al. (1982) used tracer techniques incorporating particles and film to provide significant qualitative information, but it generally suffers from poor spatial resolution and generally provides lagrangian information where an eulerian perspective is desirable. The air entrainment associated with the free surface instability of breaking waves also inhibits these methods, particularly near the water surface. Jansen (1986) used fluorescent tracers and ultraviolet light to view particle trajectories in the aerated region of breaking waves, yet these measurements still suffer from the other previously mentioned shortcomings. More recently several investigators have employed velocity measurement using Laser Doppler Anemometry (LDA). Stive (1980) and Nadaokah and Kondoh (1982) have contributed some of the early significant data sets using this technique in the surf zone. LDA offers very high precision and spatial resolution but the time it requires generally precludes any truly synoptic measurements of the flow

[1] Engineer, Taylor Engineering, Inc., 9086 Cypress Green Drive, Jacksonville, FL 32256, U.S.A. (formerly Graduate Assistant, Department of Coastal and Oceanographic Engineering, University of Florida).
[2] Assistant Professor, Department of Coastal and Oceanographic Engineering, University of Florida, Gainesville, FL 32611, U.S.A.

field. However, the most significant drawback to LDA techniques is that the high levels of air entrainment typical of the upper surf zone cause such significant signal drop-out as to completely degrade the fidelity of the measurements in this region. For example, although Nadaoka and Kondoh (1982) provide measurements of the vertical distribution of cross-shore velocity at several stations through the surf zone, they do not provide measurements above the level of the wave trough, and aeration affects the velocity profiles below the trough in the inner reaches of the surf zone significantly. As a result even averaged quantities such as the shoreward directed mass flux (due to contributions above the wave trough level) are not measured directly but only inferred by integration of the corresponding below-trough velocity measurements. These restrictions inhibit the development of a complete picture of the vertical flow structure in this region.

DPIV THEORY

Willert and Gharib (1991) describe a system that digitally performs a process similar to the opto-mechanical method employed in particle image velocimetry. Neutrally buoyant particles are introduced into a fluid flow and video images are recorded and digitized. Sequential digital images (each frame capturing a single instance in time) are analyzed using frequency domain techniques. After digitizing, small sections of each image, called areas of interest (AOIs), are compared. The AOIs represent identical locations on each consecutive image.

Willert and Gharib used the mathematical definition of cross-correlation in the frequency domain

$$\Phi_{fg}(u,v) = F^*(u,v) \times G(u,v) \tag{1}$$

where F* is the complex conjugate of the Fourier transform of f(m,n) and G(u,v) is the Fourier transform of g(m,n). They employed fast Fourier transforms (FFT) to reduce processing time. After finding Φ, they performed an inverse FFT to return the data to the spatial domain.

Essentially the process tries to match the pattern found in the first AOI with that in the second after the pattern has shifted. The location of the peak value of the cross-correlation function represents the point that best correlates the particle positions in each AOI. The shape of the peak value depends on the noise level. Large amounts of noise tend to broaden the peak. Smaller peaks also occur due to some correlation between incorrect particle pairings. However, the maximum value found in ϕ_{fg} indicates the best correlated displacement over the AOI. Particles generate noise as they move out of the AOI laterally, vertically or normal to the plane of view. Assumably the AOI is large enough to allow a majority of the particles in the first AOI to appear in the second. Figure 1 shows a typical example resulting from the application of the correlation technique for particles settling in the +y direction.

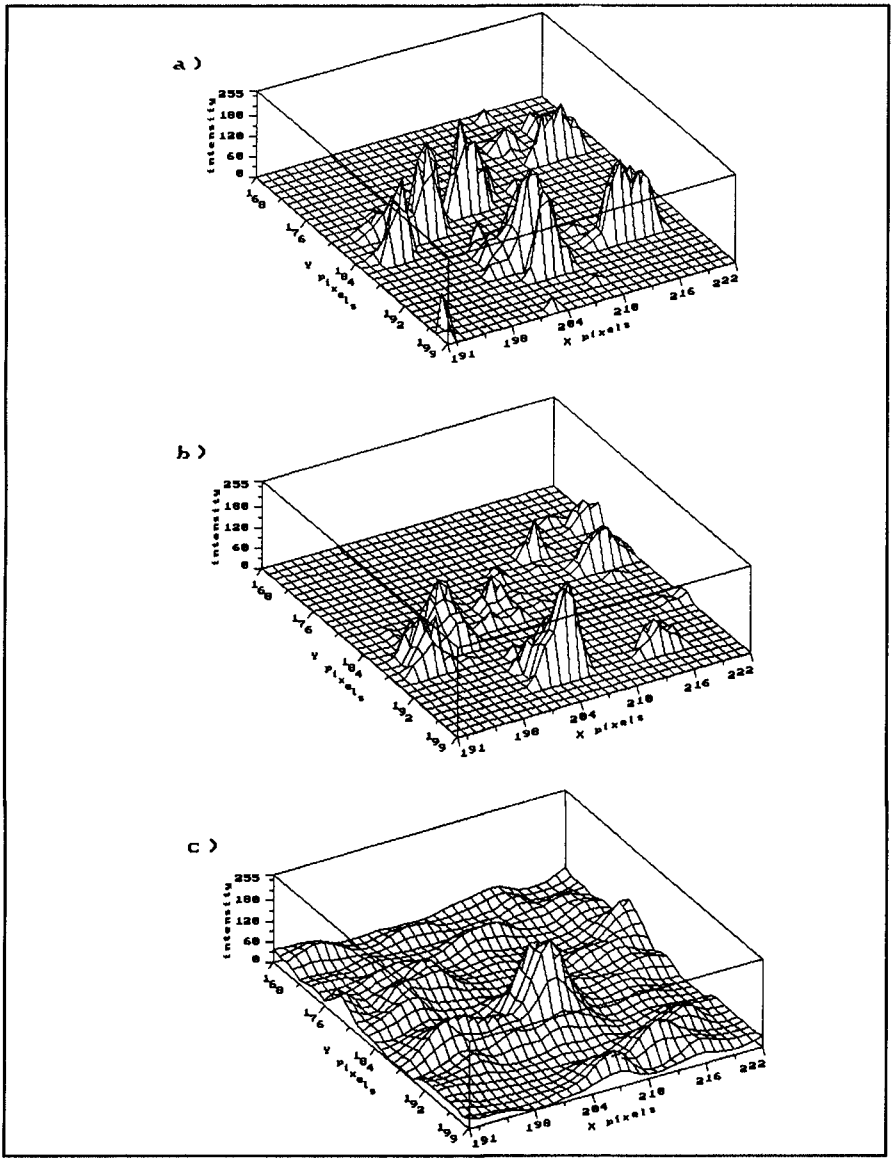

Figure 1 Graphical representation of pixel intensities within an area of interest in a) image 1 and b) image 2 and c) the inverse transformed correlation peak in the spatial domain. The maximum peak in c) indicates a displacement of approximately 4 pixels in the +y direction (downward).

Two different centroiding techniques may then be employed to examine the peak. A center of mass method (Kimura and Takamori, 1986) provides one pixel accuracy but depends on the threshold value used to determine the limits of the peak. The method Willert and Gharib suggest provides sub-pixel accuracy. In controlled experiments, they found a minimum uncertainty value of 0.01 pixels. However, in practice the uncertainty may reach an order of magnitude higher. The peak and each of the two neighboring data points are fitted with parabolic curves in both the vertical and horizontal directions. The distances from the origin to the location of the maxima of these parabolas determine the displacement vector to sub-pixel accuracy. Dividing the displacement vector by the known time difference between frames provides the velocity vector.

EXPERIMENTAL SETUP

All experiments were carried out by the authors at the University of Florida's Coastal and Oceanographic Engineering Laboratory in Gainesville, Florida, USA. Waves were generated in the multifunctional wave flume equipped with plate glass panels running the entire length on both sides providing flexible access to camera and lighting positions. Wave data were collected using a capacitance type wave gauge. Six separate tests were run: tests 1, 2, and 3 in approximately 30 centimcters of water and tests 4, 5, and 6 in approximately 23 centimeters of water. For each test series at a specific water depth, the wave periods varied from 0.85 to 2.13 seconds. The video tape and wave data were then analyzed to determine velocity fields, mean watcr level set-up and wave height distributions.

All video imaging employed gray scales rather than color because gray scales provide a higher spatial resolution and tangibly greater light sensitivity. Gray scale video equipment also costs substantially less than similar quality color equipment. The advantage of gray scale imaging is realized during proccssing because DPIV relies on pixel intensity values to distinguish particles. Color docs not offer any advantage over gray scale for this process.

Mulifunctional Wave Flume

The internal wave flume—approximately 28 meters long, 58 centimeters wide and 1.4 meters deep—is equipped with both a flap type and piston type wave maker. The smaller Seasim RSP 60-20 Modular Piston Wave maker used during the experiments is computer controlled through a central electronic system with feedback loops to minimize reflections and generation of free second harmonics. The wave maker produced monochromatic waves propagating towards a fixed beach with slope 1 on 20. The horizontal bottom portion of the flume extends 15 meters from the wave maker. The fixed beach slope then extends for another 10 mcters. The flume also comes with a remotely controlled carriage capable of transiting its entire length. A capacitance type wave gauge was attached to the movable carriage and cabled to a data acquisition computer.

Video equipment used at the experiment site included a Panasonic WV-5470 high resolution gray scale video monitor, a Panasonic AG-1970 super-VHS recording

VCR, and a Vicon VC2400 high resolution gray scale CCD video camera with variable shutter speed. The camera provides 570 lines of horizontal resolution (which is actually above super-VHS quality) and requires only 0.2 lux minimum illumination. Shutter speeds range from continuously open to 1/10,000 of a second. A shutter speed of 1/1,000th of a second minimized blurring of the particles and still allowed sufficient light to pass through the camera lens for adequate videotaping. Both zoom and wide angle lenses were available for use. Lens magnification depended upon the wave characteristics at each particular camera location. The goal was to fill the view with as much of the flow field as possible to maximize resolution during processing. Ambient light was controlled by placing a light shield made of flexible polyurethane coasted nylon fabric around the position of the video camera and flume. The light shield covered three panes of glass and could be positioned anywhere along the flume. Removable side panels on the light shield provided access to the camera when necessary. All video was recorded on master quality double coated super-VHS video tapes.

The moveable chassis was equipped with the following items: a light source, a cylindrical focusing lens and a dispenser for the neutrally buoyant particles. The light source was a 500 watt electric bulb enclosed in a wooden box with a slit approximately 2 millimeters wide cut in the bottom. The slit was aligned with the long axis of the flume (i.e., direction of wave propagation) and allowed only a portion of the light from the bulb to escape the box as a quickly dispersing plane (see Figure 2 for a schematic of the experimental apparatus).

The light then passed through the cylindrical lens and focused into a tight plane perpendicular to the bottom of the flume. With the lens approximately 1 meter above the flume bottom, the focused light diffused to a width of 1 centimeter at the flume bottom. Notably the light only remained on for periods of a few minutes to minimize the chance of overheating caused by the high power consumption of the light source and the wooden box. Despite this safety precaution, the inside bottom of the box was charred by the end of the experiment. The use of a nonflammable material to construct the light box for future applications is recommended.

Pliolite, a granular material used as a road paint strengthening ingredient with a specific gravity of 1.04 was used for the neutrally buoyant particles. Bright white, Pliolite is readily visible under the lighting conditions used during the experiments. Pliolite's highly irregular shape traps a proportionately large amount of air, causing the Pliolite to remain on the water surface when first introduced. Therefore, the pliolite was first washed in liquid soap and stored under water to facilitate breaking the surface tension when the particles were introduced to the flume. Separating the fines from the pliolite left particles ranging in size from 0.5 to 2 millimeters.

The pliolite dispenser, located next to the light source, was designed to work like a hopper. A board was fixed diagonally across the inside of the dispenser to act as a chute for the released pliolite. A second hinged board was installed so that it would form a "V" with the fixed board. Two elastic bands maintained tension on the hinged board. The pliolite was placed along the intersection of these two boards and held there until being dispensed. The chute was positioned to distribute the particles

linearly near the intersection of the light plane and the water surface. The pliolite release mechanism, designed to overcome the tension of the elastic bands, was connected to the outside of the flume. Water from an elevated container located above the chassis was fed along the top of the fixed board by plastic tubing and released through a series of small holes directed down the chute. This water washed any pliolite out of the dispenser that gravity had not removed during the initial opening.

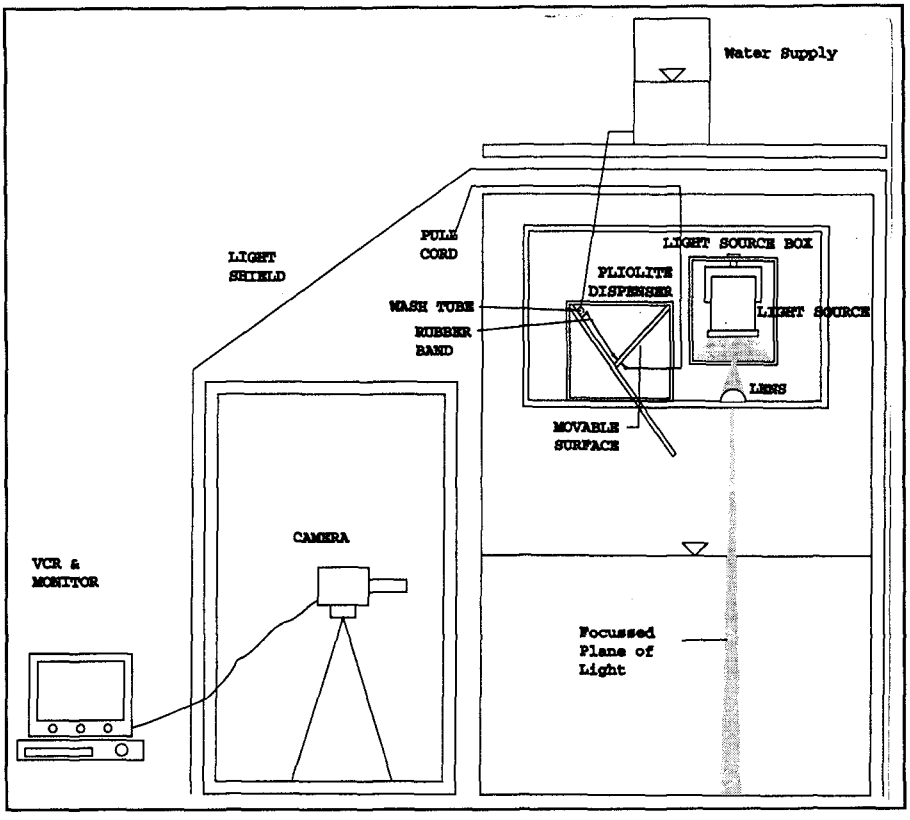

Figure 2 Experimental apparatus including video equipment location and movable chassis arrangement (cross section, long axis of tank).

To calibrate the video, a grid of 2 centimeter by 2 centimeter squares etched in clear Plexiglas was used to compensate for the magnification effects of filming through three types of media, namely air, glass, and water. Video of this grid was used to determine the number of pixels per centimeter as recorded by the camera. The bottom of the grid, tapered to the beach and held firmly to the slope, allowed the grid lines to be read vertically and horizontally.

Experiments began once the wave flume was filled to the appropriate water level and allowed to settle, after which a water depth reading was recorded from the flat portion of the flume. The wave maker then generated waves at the designated frequency. These waves were observed to determine the break point position and initial camera location. Wave gauge data were recorded along the flat portion for a deep water reading, at the beginning of the slope for initial shoaling data, and any appropriate locations outside and within the surf zone for setup and shoaling data.

The number of camera positions required for each test depended upon the field of view that could be achieved. The area from just outside the breakpoint to inside of the transition point was the focus of these experiments. The camera was placed inside the light shield at the proper location and the position of the center of the field of view along the flume was recorded. Next, the calibration grid was placed along the long axis of the flume in the field of view. The light source without the focusing lens illuminated the grid. This allowed filming the grid and minimizing any shadows the grid produced. It was found that the cylindrical lens created shadows too intense to provide any readings from the grid. The grid also allowed the camera to be focused to the proper location at the tank centerline. The pliolite was loaded into the dispenser and the flushing water source was connected to the dispenser and the focusing lens was replaced. At this point, the VCR began recording, the pliolite was released into the flume, and the light source was turned on. To produce an adequate ensemble average of flow characteristics required a minimum 30 cycles for each wave so taping lasted about two minutes for each test, at which point the light was shut off and the recording stopped. The camera was then moved to a location partially overlapping the field of view of the previous position and the process repeated until the transition point had been recorded.

When the taping ended the wave maker was stopped and the flume water level allowed to settle in order to eliminate any residual low frequency activity. Wave gauge data for still water levels were recorded for each station previously investigated. A second water level reading was taken in the flat portion of the flume to determine if any water was lost during the testing. The entire process was repeated for the next wave frequency.

DATA PROCESSING

All image digitization was carried out on a personal computer equipped with a 80486/66 MHz DX2 CPU. Computer peripheries included an EditLink 2200/TCG VCR controller card and a one megabyte frame grabber board as accessories. An image processing software package with macro language capabilities digitized and filtered the images. Several C language programs were written to control the VCR through the VCR controller card. The same super-VHS recording VCR and high resolution monitor were used during the digitization process.

The EditLink 2200/TCG can stripe a video tape with longitudinal Society of Motion Picture and Television Engineers (SMPTE) time code on one or both audio tracks. This was done after initial taping; however striping the tape before taping reduces the possibility of erasure. The EditLink manufacturers claim that the time

code can be used to locate any position on the video tape to an accuracy of +/- 1 frame. Trials of various positions on the tape confirmed this. Actually, each trial resulted in the EditLink finding the exact frame searched.

Macro files were written to automate the process of digitizing the video images by the frame grabber board. The images were processed in batches of 50. First, an image is digitized at a resolution of 640 columns by 480 lines. The 480 lines is the maximum allowable vertical resolution of the frame grabber card. A compiled C program called from the macro instructs the VCR controller card to advance the tape one frame. The next image is digitized and the process repeated. After 50 images have been digitized, a C program stops the VCR. This circumvents the automatic shut-off feature of the Panasonic AG-1970. This feature will shut the VCR off if it detects no "activity" for roughly three consecutive minutes. Unfortunately, it does not recognize frame advance as "activity." This 50 image limit actually provides an amount of data, about 15 megabytes, that most current hard disk drives can reasonably handle.

Next, the fifty images were filtered. The filtering process is based on a histogram analysis of the pixel values in each image. All pixel values lower than the 90th percentile are set to black or 0. All remaining pixels from the 90th to 99th percentile are linearly scaled from black to white (0 to 255). These filtered images were stored for later processing. A C program then directs the EditLink to find the next frame and digitizing continues.

The filtering process produced one of the most important advances in this research. Air bubbles entrained in the flow due to the breaking wave's impinging jet can be filtered out of the image. Given the lighting conditions used in the experiment, the bubbles have lower gray scale pixel intensities than do the pliolite. By visual inspection of the filterd images, the authors determined the histogram percentile range for the air bubbles and pliolite.

A Sun SPARC-LX workstation processed most of the velocity fields. The 486 microcomputer can process the velocity fields about 33% slower than the Sun workstation, so it was used to process only a small portion of the velocity fields. *Matlab*® by the Math Works, a matrix manipulation software package (also with macro language capabilities), was used to process the images on both the 486 microcomputer and the Sun workstation. All analysis of the velocity fields was done on the 486 microcomputer using this software package.

The filtered images were transferred to the Sun (or occasionally the 486) for DPIV processing. A series of M files (*Matlab*® macro language) were written to fully automate the process of analyzing the images and returning velocity fields. All data (i.e., filtered images and velocity field files) were stored on a high capacity magneto-optical (MO) disk in compressed format. The MO disk can store over 600 megabytes of data and currently contains over 200 MB of compressed velocity field data and over 300 MB of compressed filtered images.

A concern exists regarding the extent to which aeration of a broken wave crest, combined with the filtering process, may affect the velocity field determination in DPIV. The bubbles produced during wave breaking may distort the perceived

location of particles due to refraction/diffraction of the reflected light. To determine the net effect of this phenomenon, a mesh grid containing particles glued to fixed positions was videotaped in the highly aerated section of flow centered on the transition region. Velocity fields were then found for this video. In theory, particles held stationary should produce zero motion in the velocity fields. Analysis of the calculated velocity fields indicated that the distortional effects of the bubbles create a mean error of 1.0 pixels in the horizontal direction and 0.8 pixels in the vertical direction. A typical scaling scenario in the test conducted results in a converted 0.5 millimeter error in the calculated displacements.

VELOCITY FIELD RESULTS

Velocity field processing began by determining the calibration values used to convert pixels to centimeters for each camera position. This rather primitive method consisted of analyzing several frames from the grid video. Unfortunately, the grid lines were very difficult to observe in the still video frame. However, the outer edges of the grid—surrounded by an opaque paper coating—provided a known distance of 12 centimeters. The pixel columns values corresponding to the left and right edges were determined using a screen pointer and mouse. The difference of these two values divided by the 12 centimeter distance yields the horizontal calibration for that camera position. The vertical calibration was determined by multiplying the horizontal calibration by the pixel aspect ratio. Several frames were compared to evaluate the accuracy of the results. Each test showed slight variation from frame to frame due to slight grid movements on the order of one pixel. An average calibration value was selected after analyzing several frames.

All velocity field processing was done without converting from pixel displacements to actual centimeters per second velocity values. Doing so reduced the multiplicative error effects produced from numerous calculations using the less accurate length conversion from pixels to centimeters. Instantaneous displacement vectors were found in pixel units—final ensemble averages were then converted back to centimeters per second values using the calibrations taken from the recorded grid frames. Vertical and horizontal displacements were saved separately for each image pair processed. Mean flow velocity and turbulence intensities were the two principle derived quantities.

The raw velocity field data resulting from the DPIV method was analyzed using ensemble averaging techniques in an effort to separate the wave and turbulent parts of the motion. Consequently, the corresponding number of video frames per period for monochromatic waves had to be determined. Table 1 shows a summary of the values for the various tests and the relevant measured wave characteristics.

To calculate ensemble values for both mean flow and turbulence requires an appropriate value for the number of frames per cycle (i.e., wave period). Standard video records at 60 frames per second. Multiplying this value and the period and rounding to the nearest whole number yields the frames per cycle. Taking an ensemble average over all of the cycles corresponding to that point in the period then

Table 1 Experimental wave and frame data.

Test Number	Period (sec)	H_b (cm)	h_b (cm)	h_o (cm)	Frames/cycle	Total Frames Processed 30 cycles	Total Frames Processed 50 cycles
1B	0.85	4.85	4.7	31.2	51	N/A	2560
2C	1.42	6.52	4.2	30.7	85	2560	4266
3C	2.13	6.42	4.5	31.2	128	3840	N/A
4C	0.85	N/A	N/A	N/A	51	1536	2560
6A	2.13	8.86	8.4	23.2	128	3840	N/A

yields the mean velocities at each 1/60th of a second interval of the wave period. For example, to process a one second wave (corresponding to 60 frames per cycle) requires the average of frame 1, frame 61, frame 121... However, due to the limiting effect of the Nyquist frequency criterion in the DPIV method, certain sections of each velocity field are sometimes left without a value. In short, holes may exist in the data. This can occur if the area of interest contains a displacement greater than 1/3 its length. This is accounted for by keeping a running total of the number of valid values for each position in the velocity fields during the ensemble averaging. Therefore, to ensemble average 50 cycles requires independent totals for each position in the resulting velocity field. This improves the flawed values near free surfaces where small variations in the wave height produce a physical velocity value during only a few of the cycles. Care must be taken when analyzing the data near boundaries so as not to overstate the effect there. This method ensures that values within the main part of the flow are not understated as they would be if the summed values for, say, 48 cycles were actually averaged over 50 cycles. Both of the above effects become more pronounced for the longer period waves processed using only 30 cycles.

The time averaging analysis consisted of summing the ensemble averaged velocities over the entire period. Absent data are accounted for in the same manner as above. Time averaging the ensemble averaged velocity fields yields the mean flow velocities.

Turbulence was found using the ensemble averaged data for each point during the period. These values are subtracted from the instantaneous values of each velocity field used to find the ensemble average. These differences are squared and summed. Dividing the sum by a running total similar to that described above accounts for the nonexistent data. The turbulence values are then time averaged similar to the mean flow. Turbulence values are returned as squared values, their same form in the momentum conservation equations.

APPLICATION OF RESULTS

A total of 21,162 velocity fields were incorporated in the ensemble averaging during all of the tests. Actually, only 17,066 of these fields are completely independent because the fields found during the 30 cycle ensemble averaging in tests 2C and 4C were used as the first 30 cycles of the 50 cycle ensemble averaging. This allows a comparison of the effectiveness of increasing the number of cycles included in the ensemble averaging.

With the required number of digitized images known, digitization began. On average, images were digitized and fully filtered within 15 seconds. The filtered images were stored in compressed format on a magneto-optical disk and transferred to the workstation for processing. Given a sufficient data storage capacity available at the processing computer, one large data exchange will yield instantaneous velocities from the DPIV image processing method. This generally did not occur. Data transfer usually entailed transferring 200 images to the workstation while removing the previously processed velocity field files for the preceding 200 images. An example of a typical instantaneous velocity field is shown in Figure 3 (recall 1 cm is approximately 16 pixels).

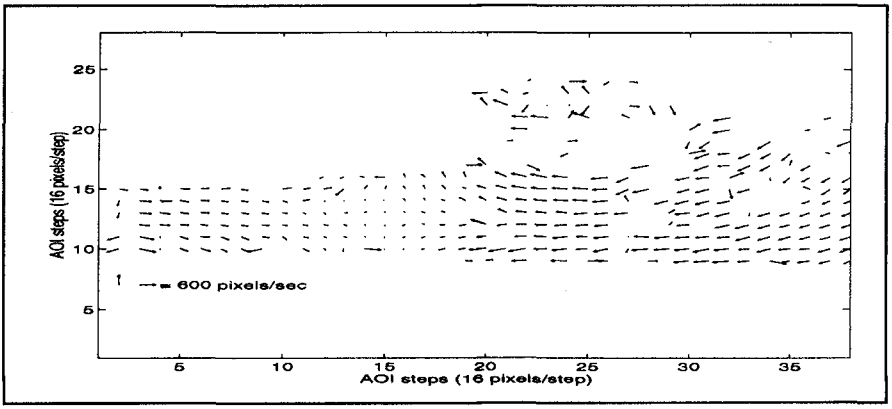

Figure 3 Instantaneous velocity field from DPIV (Test 6C, Field 536)

After acquiring all of the required instantaneous velocity fields, ensemble averaging was performed according to criteria in Table 1. As described earlier, an ensemble average of the corresponding velocity fields for each 1/60th of a second interval in the period is determined and saved. These ensemble averages, when time averaged over the period, yield results similar to Figure 4. The first image in Figure 4 shows the resultant ensemble average velocity fields of the entire field of view, including "velocities" outside the flow. A digital stopwatch superimposed on the lower portion of the screen during videotaping accounts for most of the extraneous velocities. The data in the bottom portion of the field shows the correlated motion of the stopwatch numerals. Some spurious data are also present above the flow possibly due to splashing that occurs when the jet impinges the front face of the breaking wave. Instrument noise associated with the video equipment that occurs during digitization may provide another source of non-flow velocities. All data other than the desired flow data has been removed from the second image.

Figure 5 represents an enlarged section of the middle view for the 50 cycle case in test 4C. Profiles represent typical examples of the expected flow—for the first time measurements are included above and below the wave trough elevation. In

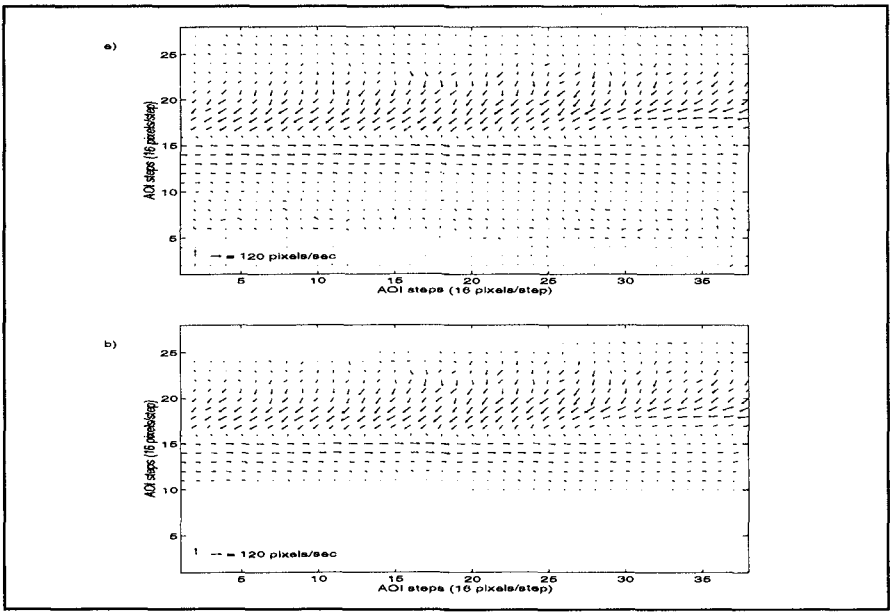

Figure 4 Ensemble time averaged velocity field with a) all non-flow data included and b) only flow related data included.

principle, mass (volume) should be conserved across any given vertical section (column) in this flow. Figure 5 indicates that mass is largely conserved in the measurements.

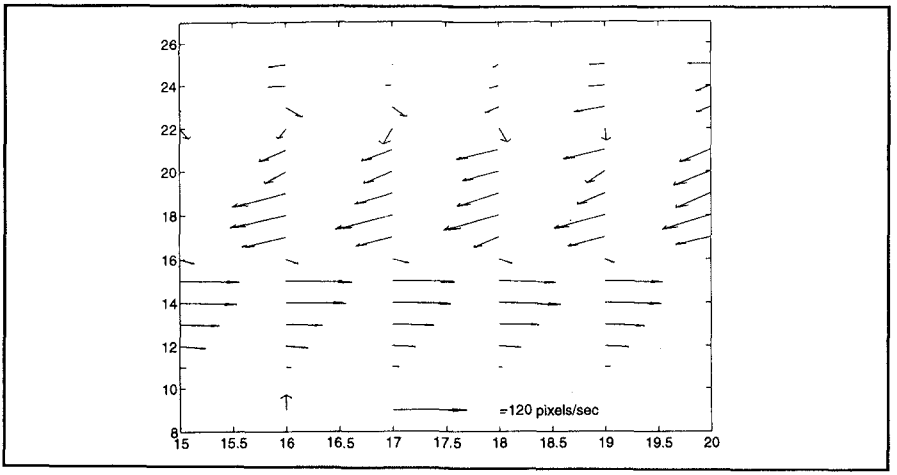

Figure 5 Columns 15-20 of ensemble, time-averaged velocity field from 50 cycle Test 6C indicating conservation of mass.

Ensemble turbulent r.m.s. velocity fluctuations are then calculated as described earlier. Observing the original video record determined the location of the relatively abrupt break in wave height change that signals the end of the transition region (or the location of the transition point). Albeit a somewhat subjective process, this technique provides greater accuracy than wave gauge data given the five centimeter gap between wave gauge stations. After determining the general location of the transition point, the average of each row in the three columns of horizontal turbulent velocity data on the offshore side of the transition point (toward the breakpoint) developed a depth varying profile of horizontal turbulent velocity fluctuations. Three column averaging thus provides two advantages: first, it further minimizes any effects that missing data may have on the ensemble averages and, second, increases the likelihood that the data represent values not only near the transition point but within the transition region. Figure 6 presents the depth varying values of the r.m.s. horizontal turbulent fluctuations (normalized by the local wave speed).

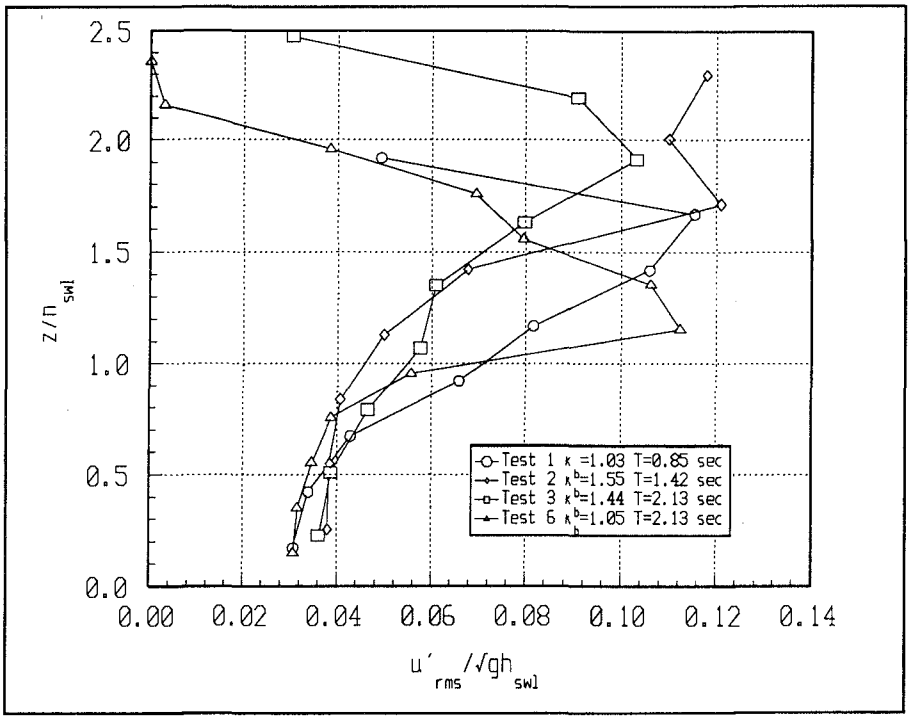

Figure 6 Dimensionless $u'_{r.m.s.}$ versus depth at the transition point.

Figure 6 shows that the below still water level (SWL) values of $u'_{r.m.s.}$ are fairly consistent within each test as well as between tests. For each test, the waves at the transition point are highly asymmetric about the SWL. This results in a majority of the crest appearing above the SWL. Mean values of the horizontal turbulent velocity

results above SWL were found and then normalized by the known breakpoint conditions.

CONCLUSION

The work presented here suggests the following:

1) Velocity measurements are now possible in the aerated crest of a broken wave within the transition region through the use of digital imaging and application of appropriate filtering techniques. The distortional characteristics of the bubbles produced during wave breaking somewhat affect the spatial resolution of these veloeities. However, the errors introduced are on the order of one millimeter per frame and, considering the fairly coarse resolution of the velocities found with DPIV, are negligible.

2) Digital particle image velocimetry provides an effective alternative to standard PIV techniques and should improve as video technology and processing speeds advance.

3) The use of video for examination of large temporal data sets by ensemble averaging provides the most efficient and economical method currently available for applications in which the temporal and spatial resolution provided by video imaging are adequate.

4) DPIV can resolve turbulent velocity fluctuations over the entire water column. However to maintain accuracy requires a high particle seeding density in the crest region.

REFERENCES

Jansen, P.C.M. (1986). Laboratory observations of the kinematics in the aerated region of breaking waves. *Coastal Engineering*, **9**, 453-477.

Nadaoka, K. and Kondoh, T. (1982). Laboratory measurement of velocity field structure in the surf zone by LDV. *Coastal Engineering in Japan*, **25**, 125-145.

Okayasu, A., Shibayama, T. and Mimura, N. (1986). Velocity field under plunging waves. *Proceedings 20th Coastal Engineering Conference*, vol. 1, 660-674.

Stive, M.J.F. (1980). Velocity and pressure field under spilling breakers. *Proceedings 17th Coastal Engineering Conference*, vol. 1, 547-566.

Wang, H., Sunamura, T. and Hwang, P.A. (1982). Drift velocity at the wave breaking point. *Coastal Engineering*, **6**, 121-150.

Willert, C.E. and Gharib, M. (1991). Digital particle image velocimetry. *Experiments in Fluids*, **10**, 181-193.